A&A 619, A73 (2018)
https://doi.org/10.1051/0004-6361/201629294

Astronomy & Astrophysics

The Solar Twin Planet Search

The age-chromospheric activity relation⋆,⋆⋆

Diego Lorenzo-Oliveira[1], Fabrício C. Freitas[1], Jorge Meléndez[1], Megan Bedell[2,7], Iván Ramírez[3], Jacob L. Bean[2], Martin Asplund[4], Lorenzo Spina[1,8], Stefan Dreizler[5], Alan Alves-Brito[6], and Luca Casagrande[4]

[1] Universidade de São Paulo, Departamento de Astronomia do IAG/USP, Rua do Matão 1226, Cidade Universitária, 05508-900 São Paulo, SP, Brazil
e-mail: diegolorenzo@usp.br
[2] University of Chicago, Department of Astronomy and Astrophysics, Chicago, IL, USA
[3] Tacoma Community College, 6501 South 19th Street, Tacoma, WA 98466, USA
[4] The Australian National University, Research School of Astronomy and Astrophysics, Cotter Road, Weston, ACT 2611, Australia
[5] Institut für Astrophysik, Universität Göttingen, Germany
[6] Instituto de Fisica, Universidade Federal do Rio Grande do Sul, Porto Alegre, Brazil
[7] Center for Computational Astrophysics, Flatiron Institute, 162 5th Ave., New York, NY 10010, USA
[8] Monash Centre for Astrophysics, School of Physics and Astronomy, Monash University, VIC 3800, Australia

Received 12 July 2016 / Accepted 20 June 2018

ABSTRACT

Context. It is well known that the magnetic activity of solar-type stars decreases with age, but it is widely debated in the literature whether there is a smooth decline or if there is an early sharp drop until 1–2 Gyr that is followed by a relatively inactive constant phase.
Aims. We revisited the activity-age relation using time-series observations of a large sample of solar twins whose precise isochronal ages and other important physical parameters have been determined.
Methods. We measured the Ca II H and K activity indices using ≈9000 HARPS spectra of 82 solar twins. In addition, the average solar activity was calculated through asteroids and Moon reflection spectra using the same instrumentation. Thus, we transformed our activity indices into the S Mount Wilson scale ($S_{\rm MW}$), recalibrated the Mount Wilson absolute flux and photospheric correction equations as a function of $T_{\rm eff}$, and then computed an improved bolometric flux normalized activity index $\log R'_{\rm HK}(T_{\rm eff})$ for the entire sample.
Results. New relations between activity and the age of solar twins were derived by assessing the chromospheric age-dating limits using $\log R'_{\rm HK}(T_{\rm eff})$. We measured an average solar activity of $S_{\rm MW} = 0.1712 \pm 0.0017$ during solar magnetic cycles 23−24 covered by HARPS observations, and we also inferred an average of $S_{\rm MW} = 0.1694 \pm 0.0025$ for cycles 10−24, anchored on a sunspot number correlation of S index versus. We also found a simple relation between the average and the dispersion of the activity levels of solar twins. This enabled us to predict the stellar variability effects on the age-activity diagram, and consequently, to estimate the chromospheric age uncertainties that are due to the same phenomena. The age-activity relation is still statistically significant up to ages around 6−7 Gyr, in agreement with previous works using open clusters and field stars with precise ages.
Conclusions. Our research confirms that Ca II H & K lines remain a useful chromospheric evolution tracer until stars reach ages of at least 6−7 Gyr. We found evidence that for the most homogenous set of old stars, the chromospheric activity indices seem to continue to decrease after the solar age toward the end of the main sequence. Our results indicate that a significant part of the scatter observed in the age-activity relation of solar twins can be attributed to stellar cycle modulations effects. The Sun seems to have a normal activity level and variability for its age.

Key words. stars: solar-type – stars: evolution – stars: fundamental parameters – magnetic fields

1. Introduction

The chromospheric activity of solar-type stars is one of the observed manifestations of a broad phenomenon called stellar magnetic activity, which is expected to be driven by the same physical principles as the solar dynamo. The paradigm is that the complex interplay between turbulent convection and rotation triggers the stellar cyclic and self-sustained global magnetic activity (Parker 1970). As the star ages, it is expected that its rotation, and consequently, its magnetic activity, decreases due to angular momentum loss through magnetized winds and structural variations on evolutionary timescales.

⋆ Based on observations collected at the European Organisation for Astronomical Research in the Southern Hemisphere under ESO programs 188.C-0265, 183.D-0729, 292.C-5004, 097.C-0571, 092.C-0721, 093.C-0409, 072.C-0488, 183.C-0972, 091.C-0936, 192.C-0852, 196.C-1006, 076.C-0155, 096.C-0499, 185.D-0056, 192.C-0224, 075.C-0332, 090.C-0421, 091.C-0034, 077.C-0364, 089.C-0415, 60.A-9036, 092.C-0832, 295.C-5035, 295.C-5031, 60.A-9700, 289.D-5015, 096.C-0210, 086.C-0284, 088.C-0323, 0100.D-0444, and 099.C-0491.
⋆⋆ Tables 1 and 2 are only available at the CDS via anonymous ftp to cdsarc.u-strasbg.fr (130.79.128.5) or via http://cdsarc.u-strasbg.fr/viz-bin/qcat?J/A+A/619/A73

Therefore, considering this theoretical framework, rotation (Skumanich 1972; Barnes 2007; Barnes & Kim 2010; Reiners & Mohanty 2012; dos Santos et al. 2016) and magnetic activity (Skumanich 1972; Soderblom et al. 1991; Mamajek & Hillenbrand 2008; Lorenzo-Oliveira et al. 2016b) are frequently considered as interesting clocks that are optimized for main-sequence stars of solar-type mass. Alternatively, some authors have estimated stellar ages using classical techniques such as isochrones (e.g., Ng & Bertelli 1998; Lachaume et al. 1999; Ramírez et al. 2014; Nissen 2015) and chemical abundance markers such as the Li abundance (e.g., Skumanich 1972; do Nascimento et al. 2009; Carlos et al. 2016), or, more recently, the [Y/Mg] or [Y/Al] ratio (e.g., Nissen 2015; Tucci Maia et al. 2016; Spina et al. 2016b,a). A review of different methods for estimating stellar ages is given by Soderblom (2010), who also discussed the problems affecting the different age indicators.

The first parametrization of the activity-age relation was performed by Skumanich (1972), where the chromospheric emission of the Ca II H & K lines was used as activity indicator. While there are other important magnetic activity tracers such as high-energy coronal emissions (Ribas et al. 2005; Booth et al. 1012), Mg II H & K (Oranje & Zwaan 1985; Buccino & Mauas 2008), Hα (Pasquini & Pallavicini 1991; Lyra & Porto de Mello 2005), Hβ (Montes et al. 2001), and the Ca II infrared triplet (Busà et al. 2007; Lorenzo-Oliveira et al. 2016a), the Ca II H & K lines are widely used because they are readily measurable from ground-based observatories, and also because a consistent and ready-to-use absolute flux calibration is available in the literature.

Most of the previous works suggested a smooth decrease in chromospheric activity with increasing age (Soderblom et al. 1991; Mamajek & Hillenbrand 2008; Lorenzo-Oliveira et al. 2016b), but Pace & Pasquini (2004) and Pace (2013) suggested that activity-age relations are only valid for stars younger than approximately 1.5 Gyr, with no further decay in activity after this age. The authors analyzed high-resolution UVES observations of 35 FG-type members of five open clusters spanning a wide age interval from the Hyades to M 67 and the Sun, resulting in a fit between chromospheric flux or $v \sin i$, and age. In addition, Pace (2013) assessed the age-activity diagram also through hundreds of FGK dwarfs with photometric effective temperatures and metallicities from Casagrande et al. (2011), and open clusters, to indicate a plateau after ~1.5 Gyr. This result, combining a heterogeneous sample of field stars and open clusters, is an independent confirmation of previous findings of Lyra & Porto de Mello (2005) using the Hα line, and is also in line with Pace & Pasquini (2004).

On the other hand, recent work by Lorenzo-Oliveira et al. (2016b) using dozens of M 67 (≈4 Gyr) and NGC 188 (≈6 Gyr) G dwarfs observed with Gemini North GMOS shows that the activity evolution could be extended until at least 6 Gyr. Furthermore, the authors point out that the lack of activity evolution after 1.5 Gyr could be interpreted as a mass/effective temperature and metallicity bias that affects Ca II H & K fluxes, in addition to isochronal age sample selection bias.

Therefore, the most convenient way to rule out the effects of other variables on Ca II activity levels (Rutten & Schrijver 1987; Rocha-Pinto & Maciel 1998; Gray et al. 2006; Lovis et al. 2011; Lorenzo-Oliveira et al. 2016a), minimizing biases in the age-activity correlation, is the study of chromospheric activity evolution of open clusters members (Soderblom et al. 1991; Mamajek & Hillenbrand 2008), wide binaries (Garcés et al. 2011; Desidera et al. 2006), or field stellar twins with similar mass and metallicity. In this work we adopted the last option, reassessing the age-chromospheric activity relation using a large sample of solar twins (Ramírez et al. 2014). These stars are very similar to the Sun, since their stellar parameters ($T_{\rm eff}$, $\log g$, [Fe/H]) are roughly within ±100 K, ±0.1 dex, ±0.1 dex of the solar values[1]. As the stars have very similar physical properties (mass and metallicity), the main parameter affecting changes in stellar activity is their ages. In a broader context, the magnetic activity history of our Sun is important for planetary habitability (Ribas et al. 2005; Airapetian & Usmanov 2016; do Nascimento et al. 2014) and to constrain dynamo models (e.g., Karak et al. 2014; Pipin & Kosovichev 2016).

This paper is organized as follows: Sect. 2 describes our working sample and the procedures we adopted to build a new Ca II H & K chromospheric activity index. We also investigate the solar activity variability in comparison to solar twins. In Sect. 3 we describe the derivation of isochronal ages for the entire sample and revisit the age-activity relation. The discussion of our results is presented in Sect. 4. The summary and conclusions are drawn in Sect. 5.

2. Data, measurement, and calibration

2.1. Working sample

Our sample was selected from the 88 solar twins presented in Ramírez et al. (2014). From this sample, we obtained data for 70 stars with the HARPS instrument (Mayor et al. 2003) at the 3.6 m telescope at the La Silla Observatory, to search for planets around solar twins (program 188.C-0265, Bedell et al. 2015; Meléndez et al. 2015, 2017). Additional data for 12 stars were found in the ESO archive, as detailed in Table 1. The high quality and cadence time-series observations, combined with the excellent instrumental stability of the HARPS spectrograph, enable exploring the limits of chromospheric age-dating using Ca II lines.

To measure the solar activity index, we used spectra from Ceres, Europa, Vesta, and the Moon (ESO projects 60.A-9036, 60.A-9700, 086.C-0284, 088.C-0323, 092.C-0832, 096.C-0210,289.D-5015,295.C-5031, and 295.C-5035) and correlated them with the International Sunspot Number from WDC-SILSO (version 2.0), Royal Observatory of Belgium, Brussels[2].

2.2. Contamination of spectroscopic binaries

We have visual and spectroscopic binaries in our sample, as listed in Table 2. The evolution of spectroscopic binaries may be different from that of other stars because, in principle, the interaction with its partner can change the angular momentum and consequently the chromospheric activity, so that they were ignored in the age-activity analysis. We cross-matched our sample with the subsample of spectroscopic binaries analyzed by dos Santos et al. (2017), Tucci Maia et al. (2016), and Fuhrmann et al. (2017). In addition, we removed the remaining stars with companions within 4", according to these studies. In total, 21 stars fell in these selection criteria: HIP6407, HIP14501, HIP18844, HIP19911, HIP30037, HIP54102, HIP54582, HIP62039, HIP64150, HIP64673, HIP65708, HIP67620, HIP72043, HIP73241, HIP79578, HIP81746, HIP83276, HIP87769, HIP103983, HIP109110, and HIP116906. Some of the spectroscopic binaries show higher rotation velocities than expected for their ages (dos Santos et al.

[1] $T_{\rm eff}^{\odot} = 5777$ K, $\log g^{\odot} = 4.437$, as adopted in Ramírez et al. (2014).
[2] http://www.sidc.be/silso

2016, 2017). To name a few cases, HIP67620 has also been identified as anomalously high in [Y/Mg] (Tucci Maia et al. 2016), which is interpreted as evidence of mass transfer from a former AGB companion. This transfer causes a rejuvenation in stellar activity due to transfer of angular momentum. This star is probably a solar twin blue straggler, like HIP10725 (Schirbel et al. 2015). The stars HIP19911 also has high Y abundances for its age (Tucci Maia et al. 2016), suggesting a link to the blue straggler phenomenon.

2.3. Calibration to the Mount Wilson System

The Ca II H and K activity indices were calculated from HARPS spectra following the Mount Wilson (MW) prescriptions presented in Wright et al. (2004). We compared our $S_{\rm HARPS}$ index for the entire sample of solar twins against their respective $S_{\rm MW}$ found in the literature (Duncan et al. 1991; Henry et al. 1996; Wright et al. 2004; Meléndez et al. 2009; Jenkins et al. 2011; Ramírez et al. 2014). In order to provide a more reliable calibration, a subsample of solar twins with the lowest $S_{\rm MW}$ uncertainties ($\sigma \leq 0.012$) were selected, excluding the Sun. From this subsample, our S index measurements were converted into the MW system, resulting in the following transformation equation:

$$S_{\rm MW} = 0.9444\, S_{\rm HARPS} + 0.0475, \quad (1)$$

where $S_{\rm HARPS}$ is defined as

$$S_{\rm HARPS} = 18.349\, \frac{H+K}{R+V}. \quad (2)$$

The typical standard deviation for the most inactive stars is 0.004 ($S_{\rm MW} \leq 0.190$) and 0.014, and for the active stars, it is ($S_{\rm MW} > 0.190$). For each sample star, we provide in Table 1 its $S_{\rm MW}$ collected from the literature as well as their respective ESO project identifications. The average values and standard deviation of the S values, already calibrated to the Mount Wilson system using the Eq. (1), are given in Table 2.

We tested the possibility of $S_{\rm MW}$ offsets between the observations performed before and after the HARPS June 2015 upgrade (Lo Curto et al. 2015). When we consider our $S_{\rm MW}$ calibration uncertainties, our results based on 46 stars indicate that both epochs are statistically similar, since the median $S_{\rm MW}$ absolute deviation is 0.003, which is only ~1% of their S values.

2.4. Improved activity scale for $\log(R'_{\rm HK})$ indices

From the S index, we converted into $R_{\rm HK}$, which is the total flux (F) in units of erg cm^{-2} s^{-1} at the stellar surface in the H and K lines normalized by the bolometric flux ($F_{\rm HK}/\sigma T_{\rm eff}^4$). However, $R_{\rm HK}$ has a strong photospheric contamination ($R_{\rm phot}$) that needs to be properly corrected for in order to select the chromospheric signature of the Ca II H & K lines ($R'_{\rm HK}$). Thus, as a first step, we strictly followed the prescriptions from Wright et al. (2004), who calibrated the activity measurements as a function of (B–V) color indices and $S_{\rm MW}$:

$$R_{\rm HK} = 1.34 \times 10^{-4}\, C_{\rm cf}\, S_{\rm MW}, \quad (3)$$

where

$$\log C_{\rm cf}({\rm B-V}) = 1.13(B-V)^3 - 3.91(B-V)^2 + 2.84(B-V) - 0.47. \quad (4)$$

The $C_{\rm cf}$ term is proportional to the bolometric normalized absolute continuum flux in the R and V Mount Wilson passbands, and the photospheric correction as a function of (B–V) is given by

$$\log R_{\rm phot}({\rm B-V}) = -4.898 + 1.918(B-V)^2 - 2.893(B-V)^3. \quad (5)$$

Finally, we obtained our activity indices $R'_{\rm HK}$ through Eqs. (3) and (4), and then subtracting Eq. (3) from Eq. (5):

$$R'_{\rm HK} = R_{\rm HK} - R_{\rm phot}. \quad (6)$$

The applicability of these equations is limited to late-F up to early-K dwarfs. Recently, Suárez Mascareño et al. (2015, 2016) extended the validity of $C_{\rm cf}$ and $R_{\rm phot}$ calibrations toward the M dwarf regime ($0.4 \lesssim ({\rm B-V}) \lesssim 1.9$). Astudillo-Defru et al. (2017) used theoretical spectra to extend the computation of $R'_{\rm HK}$ to the redder M dwarfs, ensuring a smooth transition between $C_{\rm cf}$ for solar-type stars and the lowest mass stars.

In order to test the consistency of our activity measurements, we cross-matched our sample with those of Lovis et al. (2011) and found 14 solar twins in common. The mean difference in $\log R'_{\rm HK}({\rm B-V})$ between the two databases (Lovis-Ours) is $\Delta \log R'_{\rm HK}({\rm B-V}) = +0.006 \pm 0.033$ dex. The *(B–V)* colors were taken mostly from the solar twin catalog of UBV photometry by Ramírez et al. (2012b) and were complemented with other values from the literature, as explained in Ramírez et al. (2014). We did not correct for reddening because most of our samples are located within a volume around the center of a dust-free cavity (Lallement et al. 2014). The only exception is HIP114615 ($d = 103^{+22}_{-15}$ pc), which is at a high Galactic latitude ($b = -68°$) and therefore has a negligible extinction, $E(B–V) = 0.020$, according to Schlegel et al. (1998), and 0.017 according to the correction by Schlafly & Finkbeiner (2011) or 0.008 adopting the correction proposed by Meléndez et al. (2006).

Equations (4) and (5) use the (B–V) color to calculate the photospheric and chromospheric contributions of Ca II H & K lines, which is a disadvantage, but these are directly related to $T_{\rm eff}$ and [Fe/H] rather than (B–V) (Rocha-Pinto & Maciel 1998; Lovis et al. 2011; Lorenzo-Oliveira et al. 2016b). In order to minimize these degeneracies, we therefore recalibrated the MW system by replacing the (B–V) for $T_{\rm eff}$. To do so, we cross-matched the 72 stars of Noyes et al. (1984) with those of Ramírez et al. (2013). This subsample covers a wide range of $T_{\rm eff}$, from 4350 K up to 6500 K. Thus, we investigated a new relation between $R_{\rm phot}$ (Noyes et al. 1984, Table 1) and $T_{\rm eff}$ (Ramírez et al. 2013; plotted in Fig. 1):

$$\log R_{\rm phot}(T_{\rm eff}) = -4.78845 - \frac{3.70700}{1 + (T_{\rm eff}/4598.92)^{17.5272}}. \quad (7)$$

After this, we calibrated the $C_{\rm cf}$ as a function of $T_{\rm eff}$ using the values found in Rutten (1984), excluding the giant stars. In total, 52 stars in the original Rutten (1984) sample were cross-matched with those from Ramírez et al. (2012a, 2013). The calibration followed (plotted in Fig. 1)

$$\log C_{\rm cf}(T_{\rm eff}) = (-1.70 \times 10^{-7})\, T_{\rm eff}^2 + (2.25 \times 10^{-3})\, T_{\rm eff} - 7.31. \quad (8)$$

Figure 2 shows that both approaches are strongly correlated to each other. The only significant difference appears as we consider progressively more inactive stars, where the classical MW activity indices seem to decrease their sensitivity to small activity variations, as evidenced by our new approach. Therefore, we

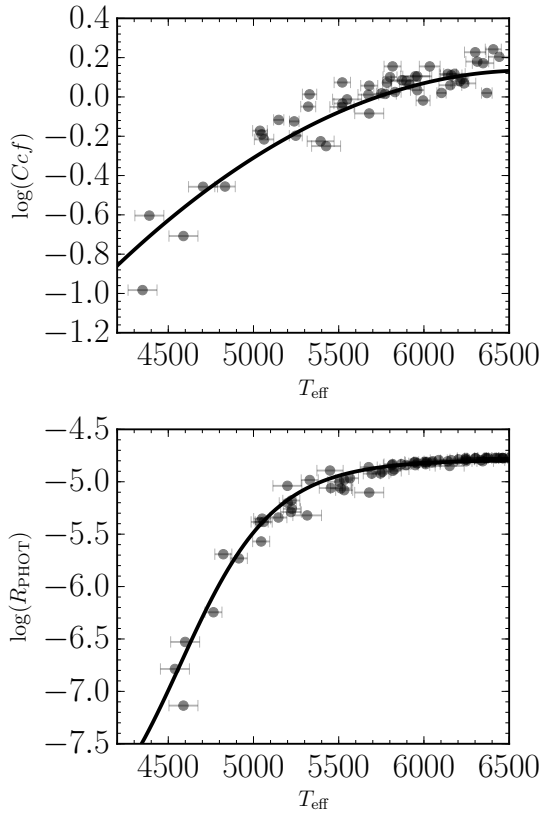

Fig. 1. *Upper panel*: C_{cf} of the stars cited in Rutten (1984). The black line represents our fit described in Eq. (8). *Lower panel*: log R_{phot} of the stars from Noyes et al. (1984). The black line represents our fit as described in Eq. (7).

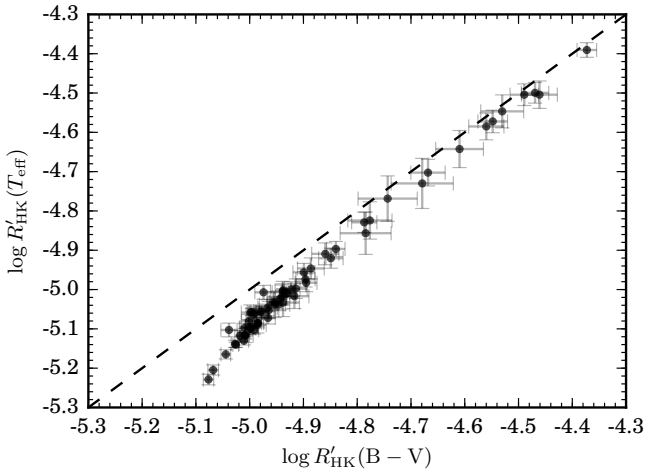

Fig. 2. $\log(R'_{HK})$ using (B–V) vs. the $\log(R'_{HK})$ using the T_{eff}. The error bars represent the intrinsic dispersion of the multiple observations. The black traced line represents the 1:1 relation.

expect that the $\log R'_{HK}(T_{eff})$ is a better indicator of activity evolution of most inactive and old stars. The use of B–V color probably collapses the effective temperature and metallicity effects, which might give more direct information about the absolute continuum flux distribution (see, e.g., Lorenzo-Oliveira et al. 2016a). This effect is more evident in inactive stars where the chromospheric/photospheric contrast is weaker.

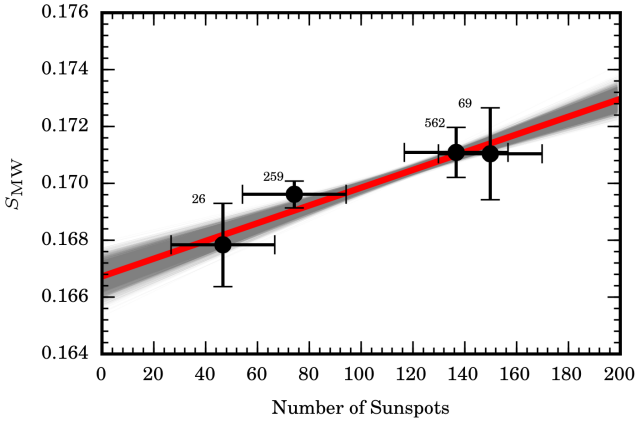

Fig. 3. Measured S index against the international sunspot number (WDC-SILSO) on approximately the same day. The red line represents the best fit between them, as presented in Eq. (9). The gray lines are the bisector regression fitting of 10^5 Monte Carlo simulations based on the activity dispersion in each sunspot number bin. The numbers placed on the top of each error bar represent the number observations that were considered to estimate its mean and dispersion.

2.5. Activity variability of the Sun and solar twins

It has been shown by Bertello et al. (2016) that the disk-integrated Ca II index has a strong linear correlation with sunspot number, although the Ca II line fluxes are expected to be better correlated to solar plages. In any case, solar plages and the presence of sunspots are different manifestations of the same underlying phenomena (namely magnetic activity) and are therefore exptected to be related in some way. We might therefore perform a calibration between the S-index and sunspot number, allowing us to increase our time baseline, to obtain a more accurate average S-index. For each day that the S-index was measured, we related it with the mean between the number of sunspots one day earlier and one day after the observation, using the WDC-SILSO sunspot numbers. In Fig. 3 we show the correlation between our S_{MW} and sunspot number. The sunspot number and the activity measurements were binned into four intervals of 40 sunspots each with their respective average (in activity and sunspot number) and dispersion represented by the error bars. Through 10^5 Monte Carlo simulations, assuming Gaussian error distribution, we derived a mean relation between the solar activity and sunspot number, followed by its respective uncertainties:

$$S_{MW} = (3.12 \pm 0.28) \times 10^{-5}\, N + (0.1667 \pm 0.0003), \quad (9)$$

where N is the international sunspot number defined by the Royal Observatory of Belgium. The internal error of this approach is $\sigma_{S_{MW}} = 0.00038 \pm 0.00009$. This relation allowed us to estimate the solar activity level in cycles 10–24 (1856–2017, see Fig. 4). We found $\langle S_{MW}\rangle(10-24) = 0.1694 \pm 0.0024$ (± 0.0004, from Eq. (9)). To check the consistency of our reconstructed solar activity history, we restricted our predictions to cycles 15–24, which were also analyzed by Egeland et al. (2017), who found $\langle S_{MW}\rangle(15-24) = 0.1694 \pm 0.0020$. Our result of $\langle S_{MW}\rangle(15-24) = 0.1696 \pm 0.0025$ indicates a similar mean activity level and dispersion in these cycles, confirming the overall consistency of our approach. We also averaged cycles 23–24 activity measurements from HARPS observations of the Moon and the other solar-system bodies (Ceres, Vesta, and Europa, hereafter SSB). The differences between them were negligible ($\langle S_{MW}\rangle^{Moon} = 0.1714 \pm 0.0011$

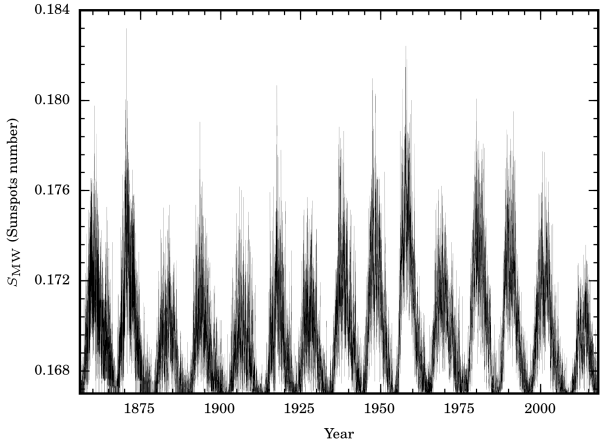

Fig. 4. Daily solar S index (using Eq. (9)) since 1850. Solar chromospheric cycles 10–24 reconstructed from the relation between S_{MW} vs. number of sunspots (see Fig. 3).

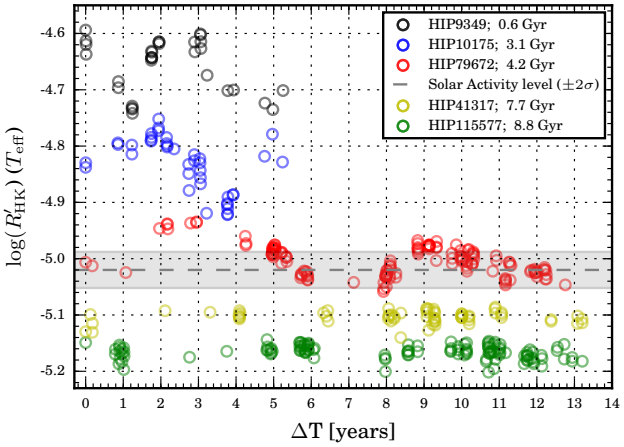

Fig. 5. Solar twin activity modulations over the years of observations. The gray dashed line and filled area correspond to the mean Sun $\log R'_{HK}(T_{eff})$ level and its fluctuations within $\pm 2\sigma$, respectively. Each circle is the nightly averaged level of activity for multiple observations.

and $\langle S_{MW}\rangle^{SSB} = 0.1706 \pm 0.0027$), therefore we combined all available spectra in order to obtain a more consistent measurement of the solar activity level ($\langle S_{MW}\rangle^{SSB+Moon} = 0.1712 \pm 0.0017$). This result derived from HARPS spectra also agrees with our predictions for $\langle S_{MW}\rangle(10-24)$. For an extensive discussion of S_{MW} determinations and calibration issues among different authors and instruments, see Egeland et al. (2017); in this context, our results for the Sun are accurate, as its measurements were made with the same instrumentation as for the stars calibrated into the MW scale.

In Fig. 5, a few illustrative cases of stellar chromospheric variability as a function of age are shown. According to our data, the amplitude of activity variations tends to decrease toward older and inactive stars. Interestingly, the well-known solar twin HIP79672 (Porto de Mello & da Silva 1997; Meléndez et al. 2014, red circles) shows a cycle modulation and amplitude that resembles those of the Sun (gray shaded region).

It is well known that the amplitude of cycle modulations of cool stars is roughly related to their activity levels (Baliunas et al. 1995; Suárez Mascareño et al. 2015, 2016; Egeland et al. 2017), which, for instance, should depend on their

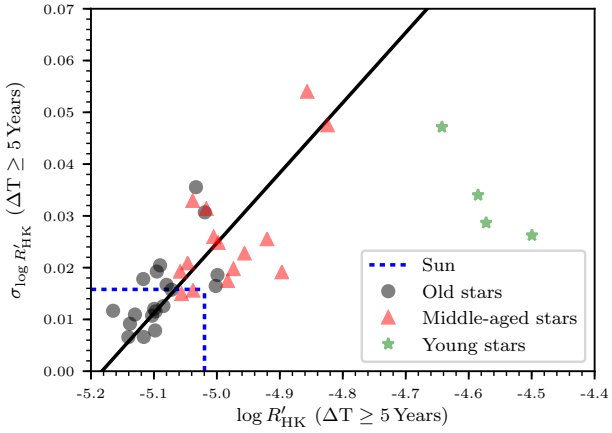

Fig. 6. $\sigma_{\log R'_{HK}(T_{eff})}$ vs. $\log R'_{HK}(T_{eff})$ relation for stars monitored for more than five years. The solid black line is the best fit. Green stars, red triangles, and black circles are solar twins with ages $t \leq 2$ Gyr, $2 < t \leq 6.5$ Gyr, and $t > 6.5$ Gyr, respectively. The blue dashed line stands for solar activity mean and dispersion.

evolutionary state (Reiners & Mohanty 2012; Schröder et al. 2013; Mittag et al. 2016). In this sense, we found in our sample that the standard deviation of $\log(R'_{HK})$ ($\sigma_{\log(R'_{HK})}$, possibly a proxy of the activity cycle amplitude) due to long-term variations increases toward active stars (Fig. 6). In order to have a more reliable estimate of $\sigma_{\log(R'_{HK})}$, it is important to monitor the whole activity cycle, but this is likely not the case for most of our sample stars. Thus, we stress that in some cases our derived $\sigma_{\log(R'_{HK})}$ can only represent a lower limit of the realistic R'_{HK} variation during the course of the activity cycles. Nevertheless, we are continuously monitoring the cycle modulations of these solar twins over the years, and in the future, we expect to provide a more robust estimate of $\sigma_{\log(R'_{HK})}$ as a function of different activity levels.

In Fig. 6 we separated our stars into three different groups: 1) young solar twins with ages younger than 2 Gyr were assigned green stars; 2) medium-age solar twins (4.5 ± 2.0 Gyr, red triangles); and 3) old solar twins with ages greater than 6.5 Gyr (black circles). Stars with time-series observations shorter than five years were not considered in order to minimize the effect of short-cycle variations. With the solid black line, we show the linear regression relating mean activity levels $\log R'_{HK}(T_{eff})$ and activity dispersion $\sigma_{\log R'_{HK}(T_{eff})}$ fitted to the data. According to our observations, the general trend indicates that the most active stars ($\log R'_{HK}(T_{eff}) > -4.7$) are in the saturated regime of activity dispersion. Since this region is not well sampled by our observations, we preferred to rule out these stars from the fit:

$$\sigma_{\log R'_{HK}(T_{eff})} = 0.62 + 0.119 \log R'_{HK}(T_{eff}). \quad (10)$$

For instance, considering the measured solar mean activity level of $\log R'_{HK}(T_{eff}) = -5.021$, Eq. (10) predicts $\sigma^{fit}_{\log\langle R'_{HK}\rangle} = 0.023$, which is in agreement with the dispersion measured through cycles 10–24 ($\sigma^{cycles\ 10-24}_{\log\langle R'_{HK}\rangle} = 0.016$). This result is evidence that the solar variability follows the same trend as is observed in solar twins. As an example, we applied this equation to the inactive stars shown in Fig. 5. Our predictions agree with the observed activity dispersions within 0.005 dex. This relation is used in Sect. 3 to estimate the lower limits on chromospheric age dating due to cycle variability and also the role of stellar variability on the scatter observed in the age-activity relation.

In Fig. 6, young stars tend to show higher dispersion in their activity measurements, while the oldest stars exhibit the lowest activity variations. It is worth noting that the robustness of the activity measurements is a balance between the amount of detectable flux excess (after correcting for the photospheric signature) and the typical cycle activity modulations. Therefore, younger and older stars tend to show different features in the age-activity diagram. The former show high levels of activity that can be easily detectable, in contrast with their higher amplitude cycle modulations. In the case of stars with very similar atmospheric parameters, the amplitude of cycle fluctuations can blur minor mass and chemical composition effects on chromospheric indicators. On the other hand, older stars with smaller activity variations and lower flux excess are the most suitable targets to detect these effects on chromospheric indicators. These minor mass and chemical composition effects are discussed in the next sections.

3. Activity-age relation

3.1. Stellar ages

The isochronal ages of our sample were derived by comparing the observed location of each star in stellar parameter space ($T_{\rm eff}$, $\log g$, [Fe/H], [α/Fe], and V absolute magnitude) with predictions of stellar evolution theory, as computed by the Yonsei-Yale group (Yi et al. 2001; Kim et al. 2002). Our method is an extension of the procedures adopted in Ramírez et al. (2014) and Tucci Maia et al. (2016), since we included in our analysis other relevant variables that also constrain the morphology of the isochrones such as V magnitude, the trigonometric distance from GAIA DR1 and Hipparcos, and [α/Fe] information[3]. This improved isochronal age-dating approach with additional constraints results in narrower age probability distributions, and consequently, in more internally consistent age estimates. Details of this straightforward probabilistic approach are given in Spina et al. (2018).

Typically, isochrone ages of main-sequence stars are very uncertain due to poorly known luminosities, which, in some cases, stems from inaccurate distances/parallaxes, and the fact that stars evolve slowly during that stage. For solar twins, this is not a problem because the precise spectroscopic parameters ($T_{\rm eff}$, [Fe/H], $\log g$, and [α/Fe]) of the stars are statiscally combined with their luminosities. The precision of stellar ages for solar twins is as good as if not better than those obtained for slightly evolved stars, for which the isochrone method works best. Moreover, because the isochrone sets can be slightly modified to precisely match the solar parameters, the ages of solar twins can be made not only very precise, but also reasonably accurate (Meléndez et al. 2012, 2014).

In addition, more sophisticated Bayesian approaches to deriving stellar isochronal ages might be necessary to investigate the long-term evolution of heterogeneous populations (see, e.g., Casagrande et al. 2011; Grieves et al. 2018). On the other hand, because we analyze a sample of stars with very precise atmospheric parameters, the prior distribution becomes approximately constant within the uncertanties of the atmospheric parameters given by the observations (Pont & Eyer 2004). In other words, the problem converges to the traditional frequentist chi-squared fit. Moreover, Chanamé & Ramírez (2012, their Fig. 7) have shown that at least one of these approaches that uses Bayesian techniques results in ages that are only slightly offset from those computed using our simpler approach.

We note that our differential isochrone method gives an age of $4.2^{+0.3}_{-0.5}$ for 18 Sco, which agrees well with the seismic age of $3.66^{+0.44}_{-0.50}$ Gyr by Li et al. (2012). In addition, for the 16 Cyg pair of solar twins (Ramírez et al. 2011), our method predicts an age of 6.4 ± 0.2 Gyr (Tucci Maia et al. 2017), which is also close to its seismic age (average of 7.0 ± 0.1 Gyr) estimated by van Saders et al. (2016). Thus, our method seems also valid for stars of approximately solar age and somewhat older.

3.2. Activity-age relation using the updated $\log R'_{\rm HK}(T_{\rm eff})$

After averaging all multiple nightly binned activity observations together with their respective standard deviation and estimating the isochronal ages, we now analyze the age-activity diagram of solar twins. The isochronal age-dating method is not optimized for young main-sequence stars. In this region, the isochrones are clumped next to the zero-age main sequence, mapping regimes of very different evolutionary speeds. These differences are translated by a statistical approach into asymmetric probability age distributions that are tailed toward older age solutions. This means that for stars of about 1 Gyr, it can be only reasonable to constrain an upper limit for the isochronal ages. Therefore, to overcome this limitation and derive a consistent age-activity relation for younger stars, we chose to simplify our approach by assigning a typical age and activity level for this class of stars. Nine stars younger than 1 Gyr (excluding the outlier HIP114615[4]) were selected in our sample, which was classified for the sake of simplicity as a single cluster with mean activity level of $\log R'_{\rm HK}(T_{\rm eff}) = -4.54 \pm 0.09$ and a typical age of $0.60^{+0.19}_{-0.14}$ Gyr, which agrees well with the canonical age of the Hyades (Perryman et al. 1998, 0.625 Gyr) and their activity level (Mamajek & Hillenbrand 2008, $\log R'_{\rm HK}({\rm B-V}) = -4.50 \pm 0.09$). It is convenient to establish $\approx$0.6 Gyr as our lower limit to young and active stars because at this age range, according to gyrochronology relations, it is expected that stellar rotation evolution converges into a well-defined sequence that only depends on rotation, age, and mass (or a suitable proxy of it), in a first-order approach (Barnes 2007; Barnes & Kim 2010; Mamajek & Hillenbrand 2008).

In Fig. 7 (left panel), we show the age-activity relation of solar twins from 0.6 to 9 Gyr. After an extensive radial-velocity (RV) monitoring of the whole sample, dos Santos et al. (2017) detected a considerable fraction of spectroscopic binaries of 25% (21 stars, see Sect. 2.2) and an overall multiplicity fraction (taking into account the wide-binary systems) of $\approx$42%. The presence of an unresolved companion in the spectra might bias the determination of atmospheric parameters and especially the activity measurements. After the RV monitoring, we are therefore confident that our sample of isolated solar twins is suitable for the age-activity (AC) analysis. Wide binaries are visually resolved, showing large orbital separation that prevents the angular momentum transfer between the components, so that these targets can be considered as isolated stars. Our age-activity analysis is restricted to a sample of 60 single and wide-binary stars (82 stars − 21 spectroscopic binaries − HIP114615). In addition, the wide-binary star HIP77052 (angular separation of only 4.4″) was also discarded since it shows very asymmetric age error bars, a very high level of chromospheric activity for the assigned age, and chemical abundance anomalies have been reported in

[3] Except for HIP29525 and HIP109110, for which rotational ages were adopted.

[4] This peculiar star was excluded from the analysis because of its very asymmetric age error bar and low activity level.

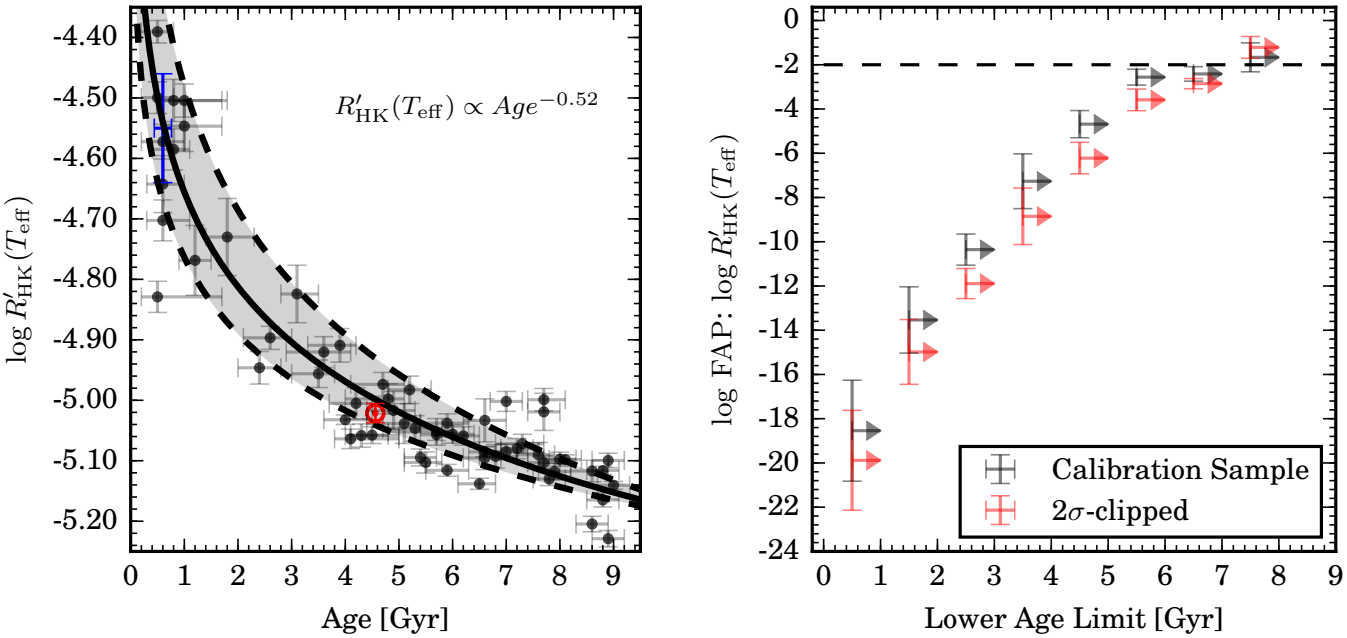

Fig. 7. *Left panel*: age-activity relation derived for solar twins. The solid line is the best fit. The Sun is plotted with its usual symbol. Stars younger than 1 Gyr are represented as a single cluster (blue error bar) with mean activity $\log R'_{\rm HK}(T_{\rm eff}) = -4.54 \pm 0.09$ and age $= 0.6 \pm 0.2$ Gyr. The shaded region is the 2σ activity variability prediction band. *Right panel*: statistical significance of the AC relation as a function of the lower age limit. Black and red symbols are the results for the entire calibration sample and after a single round of 2σ clipping removal, respectively. The false-alarm probabilities reach ≈1% around 7 Gyr.

Spina et al. (2018). As a result, the final sample used to fit the AC relation is composed of 59 solar twins spanning ages from 0.6 to 9 Gyr. For a posterior check of the solar activity behavior as a function of the other solar twins of same age, we preferred to exclude the Sun as an AC calibrator.

Different functional forms were tested to the data, and the best solution we found was a simple power-law:

$$\log(Age) = 0.0534 - 1.92 \log R'_{\rm HK}(T_{\rm eff}). \quad (11)$$

The error of the slope coefficent is 0.01 and the fractional fitting error found in age is ≈20%[5]. The estimated chromospheric age of the Sun is 4.9 ± 1.0 Gyr, and for the young cluster of solar twins, it is 0.63 ± 0.12 Gyr. It is worth noting that we avoided the young and saturated regime (ages < 0.5 Gyr). Our function is therefore valid for intermediate to old stars ($0.6 \lesssim$ ages $\lesssim 9$ Gyr), and it can be interpreted as an approximation of a more complex activity evolution that also covers the young and activity-saturated regime (Mamajek & Hillenbrand 2008).

It is convenient to estimate the effect of the cycle modulations on the AC diagram. We propagated the errors of Eq. (11):

$$\sigma^{\rm variability}_{\log(Age)} = 1.92\, \sigma_{\log\langle R'_{\rm HK}\rangle}. \quad (12)$$

This equation enables us to estimate the lower limit of chromospheric age error due to stellar cycle variability, assuming that all solar twins follow the AC trend shown in Fig. 7. The term $\sigma_{\log\langle R'_{\rm HK}\rangle}$ corresponds to the stellar variability that could be constrained through the multiple observations of our stars Eq. (10), yielding

$$\sigma^{\rm variability}_{\log(Age)} = 1.19 + 0.23 \log R'_{\rm HK}(T_{\rm eff}). \quad (13)$$

The $\sigma^{\rm variability}_{\log(Age)}$ versus $\log R'_{\rm HK}(T_{\rm eff})$ relation is not well constrained for stars more active than $\log R'_{\rm HK}(T_{\rm eff}) \approx -4.6$. In Fig. 7 (left panel), we also show the expected 2σ cycle fluctuations following the Eqs. (11) and (13). Almost all solar twins are scattered around the overall banana-like trend predicted by our AC relation, and the amplitude of the observed scatter agrees well with the predicted intrinsic cycle variability for a given age.

In order to verify the statistical significance of the AC relation, we calculated the Pearson correlation coefficient (R), setting minimum ages starting at 0 and increasing in steps of 0.1 Gyr until 9 Gyr, as shown in Fig. 7 (right panel). Then, we binned the age steps in wider intervals of 1 Gyr, estimating the mean false-alarm probability and its dispersion within each bin. Our data do not quantiatively follow the age-activity trend found by Pace (2013). The false-alarm probability around 2 or 3 Gyr is between 10^{-10}% and 10^{-7}%, respectively. For stars older than 6–7 Gyr the correlation becomes so low that the probability of a false alarm is greater than 1%. In the light of our data, we can therefore confidently say that the AC relation evolves until at least 6–7 Gyr.

On the other hand, no conclusion could be drawn about an intrinsic lack of activity evolution after this interval due to poor sampling, age uncertainties, and the possible influence of other stellar parameters on chromospheric activity levels, for example.

Still, we might go one step further and visually inspect in detail the end of the age-activity diagram isolating the variables

[5] Only two stars in our sample (HIP15527 and HIP44713) show residuals outside the 2σ domain predicted by our AC calibration. To evaluate the impact of these stars on AC calibration, we performed a single round of 2σ clipping removal and recalibrated the AC relation for the remaining stars. The slope coefficient remained constant (within ±0.01) resulting in identical chromospheric age distributions yielded by both approaches (within ≈2%).

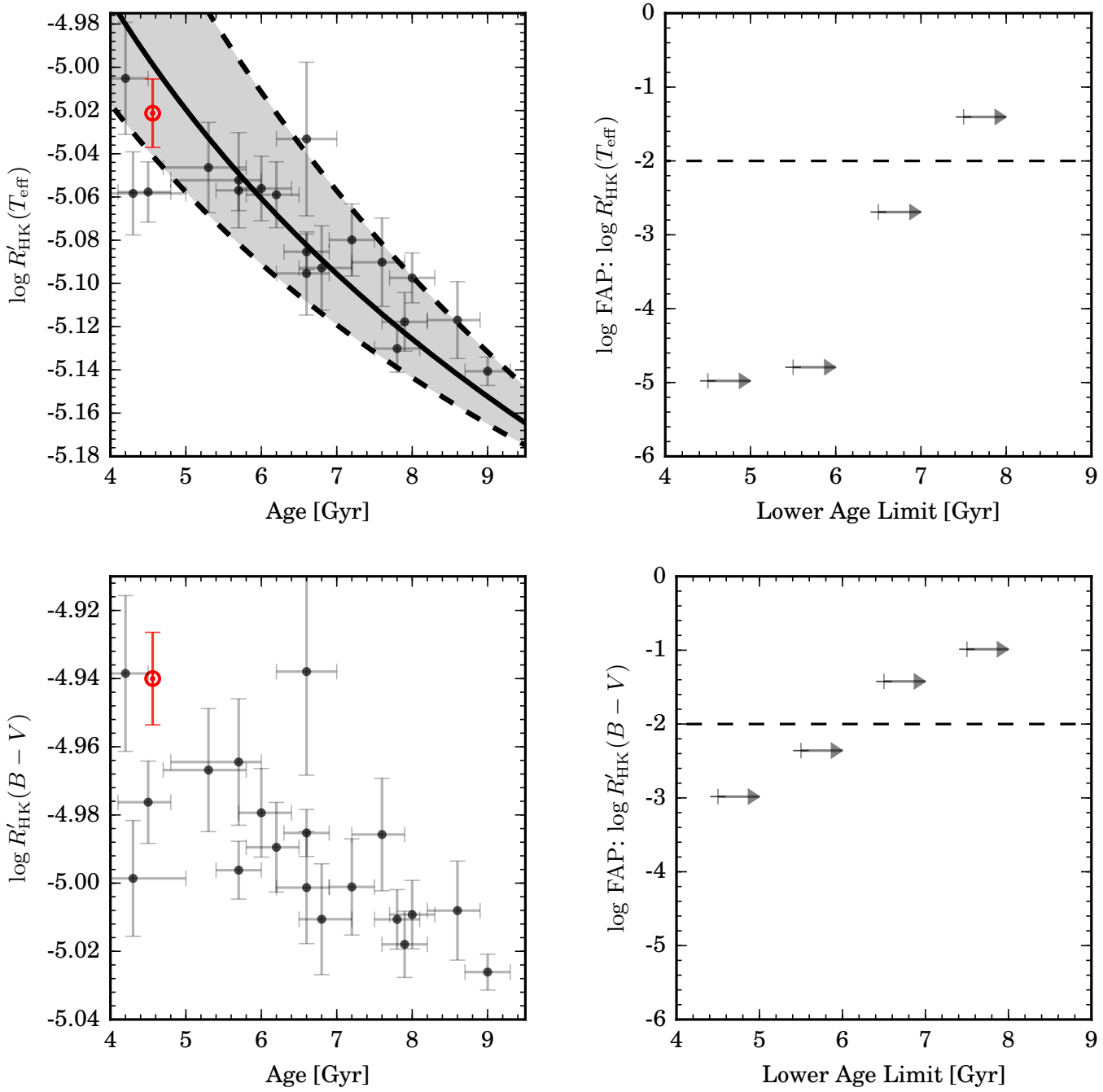

Fig. 8. *Left panels*: end of the AC relation of solar twins for $\log R'_{HK}(T_{eff})$ (*upper panel*) and $\log R'_{HK}$(B−V) (*lower panel*). The solid black line is the AC calibration from Eq. (11), and the shaded area represents the 2σ variability prediction band for $\log R'_{HK}(T_{eff})$. The Sun is plotted in red with its usual symbol. *Right panels*: same statistical analysis as in Fig. 7 applied to the best old solar twins available in our sample.

that are known to affect the activity levels of the most inactive stars such as mass, metallicity, and Ca abundances. In order to better visualize the pure effect of the AC correlation, we restricted our sample to the best old solar twins (age > 4 Gyr) available in our sample within ±0.05 of the solar values in $M/M_{\odot}$, [Fe/H], and [Ca/H] (Spina et al. 2018). In Fig. 8 (upper left panel), the end of the AC diagram is shown, followed by the predictions of Eqs. (11) and (13) for $\log R'_{HK}(T_{eff})$ activity index. The upper right panel of Fig. 8 is the same statistical analysis as in Fig. 7 (right panel), but applied only to the best old solar twins. The same statistical analysis was also repeated for $\log R'_{HK}$(B−V) activity index (lower panels), and although with a slightly lower statistical significance in comparison to the $\log R'_{HK}(T_{eff})$ versus age analysis, it is still possible to detect the activity evolution until ≈6 Gyr.

We confirmed that the AC relation also remains statistically relevant after the solar age for the most homogeneous group of stars. The typical chromospheric age error derived for these stars is ≈13% or about 1 Gyr for a typical 7 Gyr old solar twin. Possibly, the poor sampling after ≈7 Gyr together with the increasing ratio between isochronal age errors and the dynamical age range (from 7 to 9 Gyr) are responsible for the lack of

Table 3. Chromospheric age errors as a function of time-span coverage.

Minimum time-span (yr)	$\langle Age_{HK} - Age_{ISO} \rangle$ (Gyr) (Gyr)	$\langle (Age_{HK} - Age_{ISO})/Age_{ISO} \rangle$ –	Number of stars	Age^{min}_{ISO} (Gyr)	Age^{max}_{ISO} (Gyr)
≥5	-0.4 ± 0.9	16 ± 6 %	33	2.6	9.0
≥7	-0.4 ± 1.0	15 ± 4 %	23	4.2	9.0
≥10	-0.5 ± 1.0	16 ± 4 %	14	4.2	9.0
≥13	$+0.0 \pm 0.9$	13 ± 3 %	6	4.8	9.0

Notes. The AC outliers HIP15527 and HIP44713 were removed from this analysis.

statistical significance observed after this domain. In Table 3, we show the performance of our AC calibration for old stars (age > 1 Gyr) with progressively longer time-span coverage of Ca II observations (from 5 to ∼13 years). Typically, our calibration yields a chromospheric age error of about 15%, independent of time-span restrictions.

The Sun is a key target to constrain the AC relations, therefore it is important to verify whether it has a typical level and dispersion of chromospheric activity in comparison to other stars with similar parameters. Figure 7 (left panel) and Fig. 8 (left panel) show that the Sun is a normal star in comparison to other solar twins, following the overall AC trend, and it also has a compatible activity dispersion expected for a typical 4 Gyr old star.

4. Discussion

According to our results, the chromospheric activity index $\log R'_{HK}(T_{eff})$ is an interesting clock up to ≈7 Gyr. In addition to the age evolution, the chromospheric activity is well known to be also correlated with stellar mass and other atmospheric parameters such as metallicity. In this regard, our analysis using a group of stars with precise and very similar atmospheric parameters enabled us to mitigate these effects, testing the limits of the AC relation. Our analysis does not indicate that the AC relation flattens out for stars older than 1–3 Gyr, as described by Pace & Pasquini (2004) and Pace (2013). Probably the simplest explanation for the lack of chromospheric evolution in old field stars is the combination of mass/metallicity dependencies that arises from selection effects (Lorenzo-Oliveira et al. 2016b). In addition to mass effects, distant open clusters members also suffer from interstellar contamination of Ca II lines, which biases the activity measurements toward inactive levels (Curtis 2017).

If there is a sudden decrease in activity level followed by a relatively constant and inactive phase, the Rossby number versus activity diagram should reveal this behavior. In this sense, Mamajek & Hillenbrand (2008) did not find any discontinuity in the age-rotation-activity relation for stars with ages ≳1 Gyr. In addition, in the light of new open cluster data from the Kepler mission, the gyrochronology relations show very consistent results for solar-type stars from 1 to 4 Gyr old (Meibom et al. 2011, 2015; Barnes et al. 2016b). After ≈4 Gyr, the scenario of smooth rotational evolution predicted by previous gyrochronology relations is still debated. van Saders et al. (2016) combined the rotational periods of intermediate-age open cluster members and old field solar-type stars with measured rotational periods (photometric or asteroseismic rotational periods) to point out that at some threshold Rossby number, a rapid change in the topology of the magnetic fields occurs inside the star, and this effect is translated into an inefficient magnetic braking for relatively old stars. In brief, the observational effect of this change is the overabundance of unexpected old rapid rotators. According to their analysis, in the case of solar mass stars, for example, the usual gyrochronology relations therefore become ineffective for ages older than ≈4 Gyr.

In contrast, our AC diagram does not indicate any sign of discontinuity or overpresence of old and relatively rapid rotators due to an inefficient magnetic braking, assuming that activity and rotational evolutions are coupled. Barnes et al. (2016a) analyzed the Kepler sample stars with measured rotational periods and asteroseismic ages, and after removing the metal-poor and post-main-sequence stars ($\log g < 4.2$), they found a good agreement between seismic and rotational ages up to 8–9 Gyr. A similar result was previously found by do Nascimento et al. (2014), who analyzed solar analogs and candidates of solar twins from the Kepler mission. These two results are consistent with our findings in this work.

5. Summary and conclusions

The main goal of this paper is to revisit the AC relation using HARPS high-resolution time-series observations of 82 solar twins whose precise isochronal ages and other important physical parameters (such as T_{eff}, [Fe/H], $\log g$ and [Ca/H] abundances) have been obtained (Spina et al. 2018; Bedell et al. 2018). To do so, the Ca II H & K S indices were calculated following the Mount Wilson prescriptions presented in Wright et al. (2004), and then we revisited the MW calibration equations to build a new activity index $\log R'_{HK}(T_{eff})$, replacing the color index dependency by T_{eff} (Eqs. (8) and (7)). This modification mitigates the metallicity degeneracy present in (B–V) color indices.

The solar S_{MW} were also calculated from HARPS observations and were related to sunspot number (Eq. (9)). Thus, anchored on the sunspot number time-series from the Royal Observatory of Belgium, we were able to reconstruct the solar activity level in cycles 10–24 (1856–2017, $\langle S_{MW} \rangle (10-24) = 0.1694 \pm 0.0024$, which is in excellent agreement with the Egeland et al. (2017) analysis that recalibrated the solar activity level. Through multiple observations of solar twins, we detected that younger stars tend to show higher activity dispersion than older counterparts. Based on this, a simple relation between mean activity level ($\langle R'_{HK} \rangle$) and long-term activity variation ($\sigma_{\langle R'_{HK} \rangle}$) could be derived (Eq. (10)). The solar long-term activity variation follows the same trend as observed for solar twins with similar age and mean activity levels, therefore we conclude that the Sun has a mean activity level typical for its age. This relation helped us to predict the scatter due to stellar variability on the AC evolution of solar twins.

Interestingly, the AC relation found for solar twins follows the Skumanich-like function $\langle R'_{HK} \rangle \propto Age^{-0.52}$ (Eq. (11)) similar to the power-law derived by Soderblom et al. (1991). The fractional age uncertainty is approximately 20% and the AC

relation is valid only for solar-mass solar-metallicity stars with ages between 0.6 to 9 Gyr. Almost all stars in our sample are placed within the predicted AC variability band for a given age, indicating that in principle, a significant part of the observed scatter could be explained by long-term cycle modulations. For our sample, tests of statistical significance of the AC relation rule out the lack of evolution scenario after ≈2 Gyr proposed by Pace & Pasquini (2004) and Pace (2013). This means that our approach can be applied to age-date solar twins to at least 6–7 Gyr, where the false-alarm probability reaches ≈1%. Alternatively, as we consider only the best solar twins available in our sample (solar within ± 0.05 in $M/M_{\odot}$, [Fe/H], and [Ca/H]), the chromospheric activity seems to evolve monotonically toward the end of the main sequence (≈9 Gyr). This result is in line with previous works using open clusters and field stars with precise ages (Mamajek & Hillenbrand 2008; do Nascimento et al. 2014; Barnes et al. 2016a; Lorenzo-Oliveira et al. 2016a), which reinforces the use of chromospheric activity as an age diagnostic over a wide range of ages.

Acknowledgements. We would like to acknowledge the anonymous referee, whose comments have unquestionably led to an improved paper. DLO acknowledges the support from FAPESP (2016/20667-8). JM acknowledges support from FAPESP (2012/24392-2) and CNPq (Productivity Fellowship).

References

Airapetian, V. S., & Usmanov, A. V. 2016, ApJ, 817, L24
Astudillo-Defru, N., Delfosse, X., Bonfils, X., et al. 2017, A&A, 600, A13
Baliunas, S. L., Donahue, R. A., Soon, W. H., et al. 1995, ApJ, 438, 269
Barnes, S. A. 2007, ApJ, 669, 1167
Barnes, S. A., & Kim, Y.-C. 2010, ApJ, 721, 675
Barnes, S. A., Spada, F., & Weingrill, J. 2016a, Astron. Nachr., 337, 810
Barnes, S. A., Weingrill, J., Fritzewski, D., Strassmeier, K. G., & Platais, I. 2016b, ApJ, 823, 16
Bedell, M., Meléndez, J., Bean, J. L., et al. 2015, A&A, 581, A34
Bedell, M., Bean, J. L., Meléndez, J., et al. 2018, ApJ, 865, 68
Bertello, L., Pevtsov, A., Tlatov, A., & Singh, J. 2016, Sol. Phys., 291, 2967
Booth, R. S., Poppenhaeger, K., Watson, C. A., Silva Aguirre, V., & Wolk, S. J. 2017, MNRAS, 471, 1012
Buccino, A. P., & Mauas, P. J. D. 2008, A&A, 483, 903
Busà, I., Aznar Cuadrado, R., Terranegra, L., Andretta, V., & Gomez, M. T. 2007, A&A, 466, 1089
Carlos, M., Nissen, P. E., & Meléndez, J. 2016, A&A, 587, A100
Casagrande, L., Schönrich, R., Asplund, M., et al. 2011, A&A, 530, A138
Chanamé, J., & Ramírez, I. 2012, ApJ, 746, 102
Curtis, J. L. 2017, AJ, 153, 275
Desidera, S., Gratton, R. G., Lucatello, S., Claudi, R. U., & Dall, T. H. 2006, A&A, 454, 553
do Nascimento Jr., J. D., Castro, M., Meléndez, J., et al. 2009, A&A, 501, 687
do Nascimento, Jr., J. D., García, R. A., Mathur, S., et al. 2014, ApJ, 790, L23
do Nascimento, Jr., J. D., Vidotto, A. A., Petit, P., et al. 2016, ApJ, 820, L15
dos Santos, L. A., Meléndez, J., do Nascimento, J. D., et al. 2016, A&A, 592, A156
dos Santos, L. A., Meléndez, J., Bedell, M., et al. 2017, MNRAS, 472, 3425
Duncan, D. K., Vaughan, A. H., Wilson, O. C., et al. 1991, ApJS, 76, 383
Egeland, R., Soon, W., Baliunas, S., et al. 2017, ApJ, 835, 25
Fuhrmann, K., Chini, R., Kaderhandt, L., & Chen, Z. 2017, ApJ, 836, 139
Garcés, A., Catalán, S., & Ribas, I. 2011, A&A, 531, A7
Gray, R. O., Corbally, C. J., Garrison, R. F., et al. 2006, AJ, 132, 161
Grieves, N., Ge, J., Thomas, N., et al. 2018, MNRAS, 481, 3244
Henry, T. J., Soderblom, D. R., Donahue, R. A., & Baliunas, S. L. 1996, AJ, 111, 439
Jenkins, J. S., Jones, H. R. A., Tinney, C. G., et al. 2006, MNRAS, 372, 163
Jenkins, J. S., Murgas, F., Rojo, P., et al. 2011, A&A, 531, A8
Karak, B. B., Kitchatinov, L. L., & Choudhuri, A. R. 2014, ApJ, 791, 59
Kim, Y.-C., Demarque, P., Yi, S. K., & Alexander, D. R. 2002, ApJS, 143, 499
Lachaume, R., Dominik, C., Lanz, T., & Habing, H. J. 1999, A&A, 348, 897
Lallement, R., Vergely, J.-L., Valette, B., et al. 2014, A&A, 561, A91
Li, T. D., Bi, S. L., Liu, K., Tian, Z. J., & Shuai, G. Z. 2012, A&A, 546, A83
Lo Curto, G., Pepe, F., Avila, G., et al. 2015, The Messenger, 162, 9
Lorenzo-Oliveira, D., Porto de Mello, G. F., Dutra-Ferreira, L., & Ribas, I. 2016a, A&A, 595, A11
Lorenzo-Oliveira, D., Porto de Mello, G. F., & Schiavon, R. P. 2016b, A&A, 594, L3
Lovis, C., Dumusque, X., Santos, N. C., et al. 2011, ArXiv e-prints [arXiv:1107.5325]
Lyra, W., & Porto de Mello, G. F. 2005, A&A, 431, 329
Mamajek, E. E., & Hillenbrand, L. A. 2008, ApJ, 687, 1264
Mayor, M., Pepe, F., Queloz, D., et al. 2003, The Messenger, 114, 20
Meibom, S., Barnes, S. A., Latham, D. W., et al. 2011, ApJ, 733, L9
Meibom, S., Barnes, S. A., Platais, I., et al. 2015, Nature, 517, 589
Meléndez, J., Shchukina, N. G., Vasiljeva, I. E., & Ramírez, I. 2006, ApJ, 642, 1082
Meléndez, J., Asplund, M., Gustafsson, B., & Yong, D. 2009, ApJ, 704, L66
Meléndez, J., Bergemann, M., Cohen, J. G., et al. 2012, A&A, 543, A29
Meléndez, J., Ramírez, I., Karakas, A. I., et al. 2014, ApJ, 791, 14
Meléndez, J., Bean, J. L., Bedell, M., et al. 2015, The Messenger, 161, 28
Meléndez, J., Bedell, M., Bean, J. L., et al. 2017, A&A, 597, A34
Mittag, M., Schröder, K.-P., Hempelmann, A., González-Pérez, J. N., & Schmitt, J. H. M. M. 2016, A&A, 591, A89
Montes, D., López-Santiago, J., Fernández-Figueroa, M. J., & Gálvez, M. C. 2001, A&A, 379, 976
Ng, Y. K., & Bertelli, G. 1998, A&A, 329, 943
Nissen, P. E. 2015, A&A, 579, A52
Noyes, R. W., Hartmann, L. W., Baliunas, S. L., Duncan, D. K., & Vaughan, A. H. 1984, ApJ, 279, 763
Oranje, B. J., & Zwaan, C. 1985, A&A, 147, 265
Pace, G. 2013, A&A, 551, L8
Pace, G., & Pasquini, L. 2004, A&A, 426, 1021
Parker, E. N. 1970, ApJ, 162, 665
Pasquini, L., & Pallavicini, R. 1991, A&A, 251, 199
Perryman, M. A. C., Brown, A. G. A., Lebreton, Y., et al. 1998, A&A, 331, 81
Pipin, V. V., & Kosovichev, A. G. 2016, ApJ, 823, 133
Pont, F., & Eyer, L. 2004, MNRAS, 351, 487
Porto de Mello, G. F., & da Silva, L. 1997, ApJ, 482, L89
Ramírez, I., Meléndez, J., Cornejo, D., Roederer, I. U., & Fish, J. R. 2011, ApJ, 740, 76
Ramírez, I., Fish, J. R., Lambert, D. L., & Allende Prieto, C. 2012a, ApJ, 756, 46
Ramírez, I., Michel, R., Sefako, R., et al. 2012b, ApJ, 752, 5
Ramírez, I., Allende Prieto, C., & Lambert, D. L. 2013, ApJ, 764, 78
Ramírez, I., Meléndez, J., Bean, J., et al. 2014, A&A, 572, A48
Reiners, A., & Mohanty, S. 2012, ApJ, 746, 43
Ribas, I., Guinan, E. F., Güdel, M., & Audard, M. 2005, ApJ, 622, 680
Rocha-Pinto, H. J., & Maciel, W. J. 1998, MNRAS, 298, 332
Rutten, R. G. M. 1984, A&A, 130, 353
Rutten, R. G. M., & Schrijver, C. J. 1987, A&A, 177, 155
Schirbel, L., Meléndez, J., Karakas, A. I., et al. 2015, A&A, 584, A116
Schlafly, E. F., & Finkbeiner, D. P. 2011, ApJ, 737, 103
Schlegel, D. J., Finkbeiner, D. P., & Davis, M. 1998, ApJ, 500, 525
Schröder, K.-P., Mittag, M., Hempelmann, A., González-Pérez, J. N., & Schmitt, J. H. M. M. 2013, A&A, 554, A50
Skumanich, A. 1972, ApJ, 171, 565
Soderblom, D. R. 2010, ARA&A, 48, 581
Soderblom, D. R., Duncan, D. K., & Johnson, D. R. H. 1991, ApJ, 375, 722
Spina, L., Meléndez, J., Karakas, A. I., et al. 2016a, A&A, 593, A125
Spina, L., Meléndez, J., & Ramírez, I. 2016b, A&A, 585, A152
Spina, L., Meléndez, J., Karakas, A. I., et al. 2018, MNRAS, 474, 2580
Suárez Mascareño, A., Rebolo, R., González Hernández, J. I., & Esposito, M. 2015, MNRAS, 452, 2745
Suárez Mascareño, A., Rebolo, R., & González Hernández, J. I. 2016, A&A, 595, A12
Tucci Maia, M., Ramírez, I., Meléndez, J., et al. 2016, A&A, 590, A32
Tucci Maia, M., Meléndez, J., Spina, L., & Lorenzo-Oliveira, D. 2017, MNRAS, submitted
van Saders, J. L., Ceillier, T., & Metcalfe, T. S. 2016, Nature, 529, 181
Wright, J. T., Marcy, G. W., Butler, R. P., & Vogt, S. S. 2004, ApJS, 152, 261
Yi, S., Demarque, P., Kim, Y.-C., et al. 2001, ApJS, 136, 417